All-optical self-referencing measurement of vectorial optical arbitrary waveform

Chi-Cheng Chen and Shang-Da Yang*

Institute of Photonics Technologies, National Tsing Hua University, Hsinchu 30013, Taiwan
*shangda@ee.nthu.edu.tw

Abstract: We propose the Vectorial E-field Characterization Through all-Optical and self-Referenced (VECTOR) method to characterize vectorial optical arbitrary waveform with up to 100% duty cycle, which is free of ambiguity, iteration, radio-frequency or external optical reference, restriction on repetition rate, and requirement of external interferometric stabilization. The feasibility of VECTOR is experimentally verified by different waveforms created by a phase-modulated CW comb source and a built-in polarization line-by-line pulse shaper.

OCIS codes: (320.7100) Ultrafast measurements; (320.7110) Ultrafast nonlinear optics; (120.2130) Ellipsometry and polarimetry.

References and links

1. C.-C. Chen, I.-C. Hsieh, S.-D. Yang, and C.-B. Huang, "Polarization line-by-line pulse shaping for the implementation of vectorial temporal Talbot effect," Opt. Express **20**(24), 27062–27070 (2012).
2. S. T. Cundiff and A. M. Weiner, "Optical arbitrary waveform generation," Nat. Photonics **4**(11), 760–766 (2010).
3. H.-P. Chuang and C.-B. Huang, "Generation and delivery of 1-ps optical pulses with ultrahigh repetition-rates over 25-km single mode fiber by a spectral line-by-line pulse shaper," Opt. Express **18**(23), 24003–24011 (2010).
4. G. Sansone, F. Ferrari, C. Vozzi, F. Calegari, S. Stagira, and M. Nisoli, "Towards atomic unit pulse duration by polarization-controlled few-cycle pulses," J. Phys. At. Mol. Opt. Phys. **42**(13), 134005 (2009).
5. M. Aeschlimann, M. Bauer, D. Bayer, T. Brixner, S. Cunovic, F. Dimler, A. Fischer, W. Pfeiffer, M. Rohmer, C. Schneider, F. Steeb, C. Strüber, and D. V. Voronine, "Spatiotemporal control of nanooptical excitations," Proc. Natl. Acad. Sci. U.S.A. **107**(12), 5329–5333 (2010).
6. R. Trebino and D. J. Kane, "Using phase retrieval to measure the intensity and phase of ultrashort pulses: frequency-resolved optical gating," J. Opt. Soc. Am. A **10**(5), 1101–1111 (1993).
7. C. Iaconis and I. A. Walmsley, "Spectral phase interferometry for direct electric-field reconstruction of ultrashort optical pulses," Opt. Lett. **23**(10), 792–794 (1998).
8. S.-D. Yang, C.-S. Hsu, S.-L. Lin, Y.-S. Lin, C. Langrock, and M. M. Fejer, "Ultrasensitive direct-field retrieval of femtosecond pulses by modified interferometric field autocorrelation," Opt. Lett. **34**(20), 3065–3067 (2009).
9. C.-S. Hsu, H.-C. Chiang, H.-P. Chuang, C.-B. Huang, and S.-D. Yang, "Forty-photon-per-pulse spectral phase retrieval by shaper-assisted modified interferometric field autocorrelation," Opt. Lett. **36**(14), 2611–2613 (2011).
10. V. R. Supradeepa, D. E. Leaird, and A. M. Weiner, "Optical arbitrary waveform characterization via dual-quadrature spectral interferometry," Opt. Express **17**(1), 25–33 (2009).
11. H. X. Miao, D. E. Leaird, C. Langrock, M. M. Fejer, and A. M. Weiner, "Optical arbitrary waveform characterization via dual-quadrature spectral shearing interferometry," Opt. Express **17**(5), 3381–3389 (2009).
12. C.-C. Chen, Y.-S. Chen, C.-B. Huang, M. C. Chen, and S. D. Yang, "Non-iterative data inversion of phase retrieval by omega oscillating filtering for optical arbitrary waveform measurement," Opt. Lett. **38**(12), 2011–2013 (2013).
13. C. Dorrer and I. Kang, "Linear self-referencing techniques for short-optical-pulse characterization," J. Opt. Soc. Am. B **25**(6), A1–A12 (2008).
14. F. Ferdous, H. X. Miao, D. E. Leaird, K. Srinivasan, J. Wang, L. Chen, L. T. Varghese, and A. M. Weiner, "Spectral line-by-line pulse shaping of on-chip microresonator frequency combs," Nat. Photonics **5**(12), 770–776 (2011).
15. C.-C. Chen, C.-B. Huang, and S.-D. Yang, "Self-referenced frequency comb measurement by using a polarization line-by-line pulse shaper," Opt. Lett. **39**(7), 1901–1904 (2014).
16. W. J. Walecki, D. N. Fittinghoff, A. L. Smirl, and R. Trebino, "Characterization of the polarization state of weak ultrashort coherent signals by dual-channel spectral interferometry," Opt. Lett. **22**(2), 81–83 (1997).
17. T. Brixner, G. Krampert, P. Niklaus, and G. Gerber, "Generation and characterization of polarization-shaped femtosecond laser pulses," Appl. Phys. B **74**(S1), s133–s144 (2002).
18. P. Schlup, O. Masihzadeh, L. Xu, R. Trebino, and R. A. Bartels, "Tomographic retrieval of the polarization state of an ultrafast laser pulse," Opt. Lett. **33**(3), 267–269 (2008).

#223524 - $15.00 USD Received 24 Sep 2014; revised 2 Nov 2014; accepted 3 Nov 2014; published 11 Nov 2014

19. L. Xu, P. Schlup, O. Masihzadeh, R. A. Bartels, and R. Trebino, "Analysis of the measurement of polarization-shaped ultrashort laser pulses by tomographic ultrafast retrieval of transverse light E fields," J. Opt. Soc. Am. B **26**(12), 2363–2369 (2009).
20. Y. Coello, V. V. Lozovoy, T. C. Gunaratne, B. Xu, I. Borukhovich, C.- Tseng, T. Weinacht, and M. Dantus, "Interference without an interferometer: a different approach to measuring, compressing, and shaping ultrashort laser pulses," J. Opt. Soc. Am. B **25**(6), A140–A150 (2008).
21. P. Schlup and R. A. Bartels, "Impact of Measurement Noise in Tomographic Ultrafast Retrieval of Transverse Light E-Fields (TURTLE) Ultrashort Polarization Characterization," IEEE Photon. J. **1**(2), 163–171 (2009).
22. S. X. Wang, M. M. Fejer, and A. M. Weiner, "A Complete Spectral Polarimeter Design for Lightwave Communication Systems," J. Lightwave Technol. **24**(11), 3982–3991 (2006).
23. M. Ninck, A. Galler, T. Feurer, and T. Brixner, "Programmable common-path vector field synthesizer for femtosecond pulses," Opt. Lett. **32**(23), 3379–3381 (2007).
24. A. Galler and T. Feurer, "Pulse shaper assisted short laser pulse characterization," Appl. Phys. B **90**(3-4), 427–430 (2008).
25. A. M. Weiner, "Effect of Group Velocity Mismatch on the Measurement of Ultrashort Optical Pulses via Second Harmonic Generation," IEEE J. Quantum Electron. **19**(8), 1276–1283 (1983).

1. Introduction

The marriage between optical frequency combs and polarization line-by-line pulse shaping opens access to vectorial optical arbitrary waveform (V-OAW) with ultrafast evolution of amplitude, phase, state of polarization (SOP) that can span up to the entire repetition period (100% duty cycle) [1]. Scalar OAW (with static SOP) and vectorial ultrashort pulse (with small duty cycle) have been applied to radio-frequency (RF) photonics [2], intensity repetition rate multiplication of a pulse train [3], isolated attosecond burst generation [4], and selective spatiotemporal excitations with nanometer and femtosecond resolutions [5], respectively. The increased degree of freedom of V-OAW is expected to enable unique applications in ultrafast plasmonics.

A limited number of methods have been developed to measure either scalar OAW or vectorial ultrashort pulse, while none of them is readily applicable to V-OAW characterizations. The 100% duty cycle of scalar OAW prohibits the employment of conventional femtosecond pulse measurement methods requiring the generation of isolated pulse replicas [6–9]. As a result, a synchronized and well-characterized optical reference pulse [10] or a coherent RF reference wave [11–13] is often used in generating a set of interferograms, from which the relative phases of individual comb lines can be retrieved. However, the required optical or RF reference could be unavailable especially when the OAW comes from a Kerr frequency comb of large (>100 GHz) mode spacing [14]. This restriction was recently overcome by orthogonally probed dual quadrature spectral shearing interferometry (DQ-SSI) [15], where the reference probe field was produced by shaping the signal OAW itself.

To resolve V-OAW, not only the individual temporal shapes of x- and y-polarizations [i.e. the power spectra $|A_{x,y}(\omega)|^2$ and the nonlinear components of spectral phases $\phi_{x,y}(\omega)$] but their relative delay τ_{xy} and constant phase θ have to be retrieved. This can be achieved by dual-channel spectral interferometry [16, 17] if a synchronized reference optical frequency comb with known spectral phase and a bandwidth broader than or equal to that of the signal is available. It is a linear technique with high sensitivity, however, restricted by the requirement of interferometric stability (the transient SOP is vulnerable to the environmental perturbations) unless special polarization demultiplexing geometry and fast data acquisition are used [10]. Tomographic ultrafast retrieval of transverse light E-fields (TURTLE) is a nonlinear, self-referenced technique that can recover τ_{xy} and θ by using the spectrogram due to a different polarization (typically linear polarization at 45°) as the constraint for optimization [18, 19]. TURTLE is robust against interferometric perturbations but fails to measure V-OAW for a well-behaved spectrogram (surrounded by zeros) does not exist when the signal waveform is of 100% duty cycle. It was recently proposed that the data trace of multiphoton intrapulse interference phase scan (MIIPS) [20] could be used in TURTLE to recover τ_{xy} and θ [21]. This would make TURTLE applicable to V-OAW, however, it is subject to significant data redundancy, time-consuming iteration, probable sign ambiguity of τ_{xy} and θ [in the event of $|A_x(\omega)| = |A_y(\omega)|$ and $\phi_x(\omega) = \phi_y(\omega)$] [19] and has not been experimentally demonstrated in

#223524 - $15.00 USD Received 24 Sep 2014; revised 2 Nov 2014; accepted 3 Nov 2014; published 11 Nov 2014

measuring vectorial ultrashort pulse or V-OAW. In our earlier demonstration of vectorial temporal Talbot effect [1], $\phi_x(\omega)$, $\phi_y(\omega)$, τ_{xy} and θ were individually measured by optimizing the second-harmonic yields with a pulse shaper, dual quadrature spectral interferometry (DQ-SI), and monochromatic phase-scanning interferometry, respectively (please refer to Section 3.1). The 4-step approach may not be practically useful because of its high complexity, slow data acquisition, and the requirement of a well-characterized optical reference with interferometric stability.

In this paper, we report the Vectorial E-field Characterization Through all-Optical and self-Referenced (VECTOR) method that can synthesize and analytically characterize V-OAW without any external reference or ambiguity for the first time (to the best of our knowledge). It consists of one scalar OAW measurement by orthogonally probed DQ-SSI [15] and one SOP spectrum measurement by a wavelength-parallel polarimeter (WPP) [22]. The self-referenced, nearly common-path, all-optical configuration makes it robust against interferometric perturbations and compatible with Kerr frequency combs of large mode spacing. The requirement of only one nonlinear measurement (compared with three or four in TURTLE) and free of iteration or optimization greatly improve the complexity, update rate, and sensitivity of the system. The feasibility of VECTOR was experimentally verified by measuring three types of 20 GHz V-OAWs with ~2.8 ps temporal structures, but is readily applicable to >100 GHz waveforms with femtosecond local features [14].

2. Theory

The complex spectral envelope of a V-OAW can be expressed as $\boldsymbol{A}(\omega) = A_x(\omega)\boldsymbol{x} + r \times A_y(\omega) \times \exp[j(\omega\tau_{xy} + \theta)]\boldsymbol{y}$, where the bolded symbols represent vector quantities, $A_{x,y}(\omega) \equiv |A_{x,y}(\omega)| \times \exp[j\phi_{x,y}(\omega)]$ is the spectral envelope determining the temporal shape of x- or y-polarization, r, τ_{xy}, θ are the relative peak amplitude, delay, and constant phase, respectively. The overall spectral phase of the y-polarization, $\phi_{y,tot}(\omega)$, is $\phi_y(\omega) + \tau_{xy}\omega + \theta$. The first step in VECTOR is measuring $\phi_x(\omega)$ by the OAW-compatible orthogonally probed DQ-SSI [15]. Secondly, all the remaining parameters are measured by a WPP [22]. Note that WPP retrieves the frequency-dependent Stokes elements $S_i(\omega)$ (i = 0,1,2,3) by measuring the four power spectra of linear polarizations at 0°, 90°, 45°, and right-hand circular polarization $I_x(\omega)$, $I_y(\omega)$, $I_{45}(\omega) = [I_x + I_y + 2(I_xI_y)^{1/2}\cos\Delta\phi]/2$, $I_{\mathrm{RHC}}(\omega) = [I_x + I_y + 2(I_xI_y)^{1/2}\sin\Delta\phi]/2$, where $S_0(\omega) = I_x(\omega) + I_y(\omega)$, $S_1(\omega) = I_x(\omega)-I_y(\omega)$, $S_2(\omega) = 2I_{45}(\omega)-S_0(\omega)$, $S_3(\omega) = 2I_{\mathrm{RHC}}(\omega)-S_0(\omega)$, respectively. As a result, $|A_x(\omega)|$, $r|A_y(\omega)|$ and $\Delta\phi(\omega) = \phi_{y,tot}(\omega)-\phi_x(\omega)$ can be unambiguously retrieved by

$$\begin{gathered}\left|A_x(\omega)\right| = \sqrt{I_x} = \sqrt{(S_0 + S_1)/2}, r\left|A_y(\omega)\right| = \sqrt{I_y} = \sqrt{(S_0 - S_1)/2},\\ \Delta\phi(\omega) = \tan^{-1}(\frac{2I_{\mathrm{RHC}} - I_x - I_y}{2I_{45} - I_x - I_y}) = \tan^{-1}(\frac{S_3}{S_2}),\end{gathered} \tag{1}$$

form which the full vectorial field $\boldsymbol{A}(\omega)$ or $\boldsymbol{e}(t) = \mathrm{Re}\{[a_x(t)\boldsymbol{x} + a_y(t)\boldsymbol{y}] \times \exp(j\omega_0 t)\}$ can be reconstructed, where $a_x(t) = F^{-1}\{A_x(\omega)\}$, $a_y(t) = F^{-1}\{r|A_y(\omega)| \times \exp[j\phi_{y,tot}(\omega)]\}$.

3. Experiment

The experimental setup is shown in Fig. 1. A phase-modulated continuous-wave (PMCW) comb of ~17 spectral lines and 20 GHz mode spacing (50 ps repetition period) was generated by injecting a 1 kHz-linewidth CW laser (NKT Adjustik) centered at 1545 nm ($\omega_0 = 2\pi \times$ 194.17 THz) into an optical phase modulator driven by an RF tone of amplitude $1.89V_\pi$. A polarization line-by-line pulse shaper independently controlled the amplitudes and phases of the x- and y-polarized comb lines [23]. The single-source and nearly common-path configuration ensured stable τ_{xy} and θ though the carrier-envelope phase of the PMCW comb was unlocked. In the measurement of $\phi_x(\omega)$ by DQ-SSI, two probe lines spaced by 20 GHz were generated in the y-polarization [15]. The shaper output was sent to a 2-mm-thick Type II BBO for SFG, recorded by a high-resolution spectrograph and an intensified CCD camera

#223524 - $15.00 USD Received 24 Sep 2014; revised 2 Nov 2014; accepted 3 Nov 2014; published 11 Nov 2014

(Fig. 1, Path-1A). In performing WPP measurement, the shaper output was connected to a polarization manipulator (consisting of two quarter-wave plates and a polarization beam-splitter) for SOP component sampling [22]. The four power spectra $I_x(\omega)$, $I_y(\omega)$, $I_{45}(\omega)$, $I_{\mathrm{RHC}}(\omega)$ were recorded by the same spectrograph and an InGaAs detector array (Fig. 1, Path-2A).

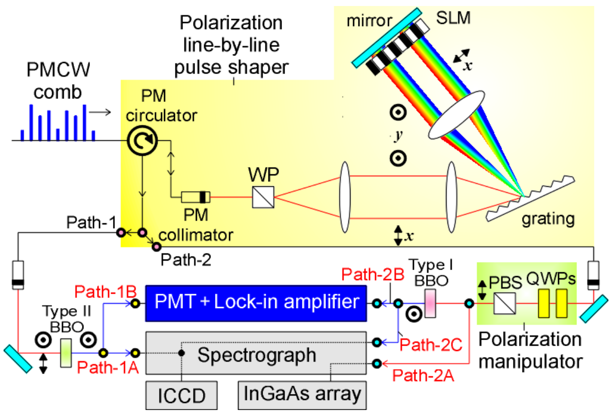

Fig. 1. Experimental setup. PM, polarization maintaining; WP, Wollaston prism; SLM, spatial light modulator; QWP, quarter-wave plate; PBS, polarization beam splitter.

3.1 Measurement of V-OAW with 100% duty cycle

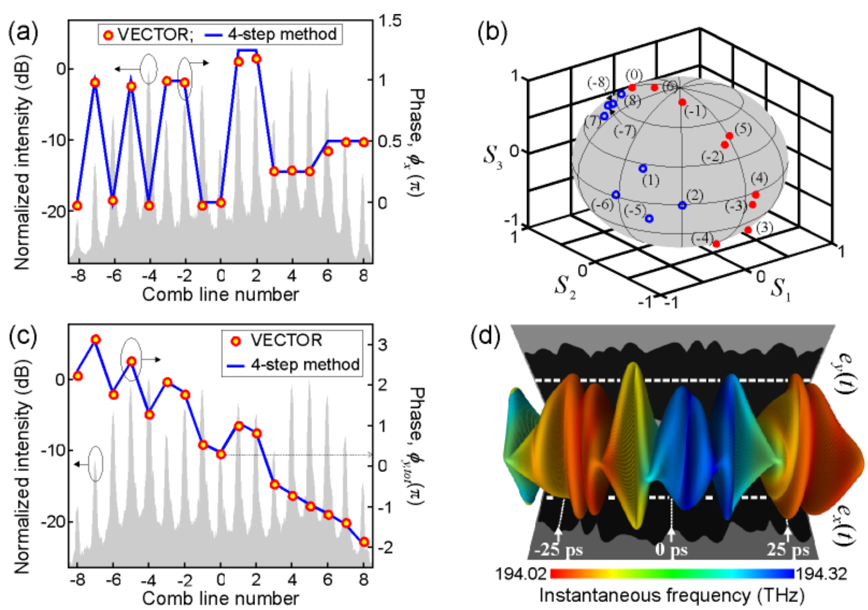

Fig. 2. The raw V-OAW measured by VECTOR. (a) Spectral intensity (shaded) and phase (circles) of $A_x(\omega)$. (b) Poincarè sphere representation of SOP. The number in parenthesis denotes the corresponding comb line number. The shadowed points are shown in open circles. (c) Spectral intensity (shaded) and phase (circles) of $r|A_y(\omega)| \times \exp[j\phi_{y,tot}(\omega)]$. (d) The quasi-3D representation of the VECTOR-reconstructed $\boldsymbol{e}(t)$. The solid lines in (a,c) represent $\phi_x(\omega)$ and $\phi_{y,tot}(\omega)$ obtained by a 4-step method.

Figure 2 shows the measurement results for a raw PMCW comb, where ϕ_x, ϕ_y change abruptly and $\Delta\phi$ mainly results from the imbalanced paths of the system. The circles in Figs. 2(a-c) illustrate ϕ_x, SOP, and $\phi_{y,tot}$ of the 17 comb lines measured by VECTOR. The reconstructed

#223524 - $15.00 USD Received 24 Sep 2014; revised 2 Nov 2014; accepted 3 Nov 2014; published 11 Nov 2014

electric field $\boldsymbol{e}(t)$ is depicted in Fig. 2(d), where the instantaneous frequencies (defined by taking the inverse of the piecewise time required for the field in passing through the maximum twice along the polarization ellipse) are displayed by different color tones. The x- and y-polarized field components, $e_{x,y}(t) = \mathrm{Re}[a_{x,y}(t) \times \exp(j\omega_0 t)]$, are independently depicted using the black projection traces onto the corresponding axes. The reconstructed $\boldsymbol{e}(t)$ clearly exhibits the signatures of V-OAW, including the time-varying SOP, strong chirp, and 100% duty cycle.

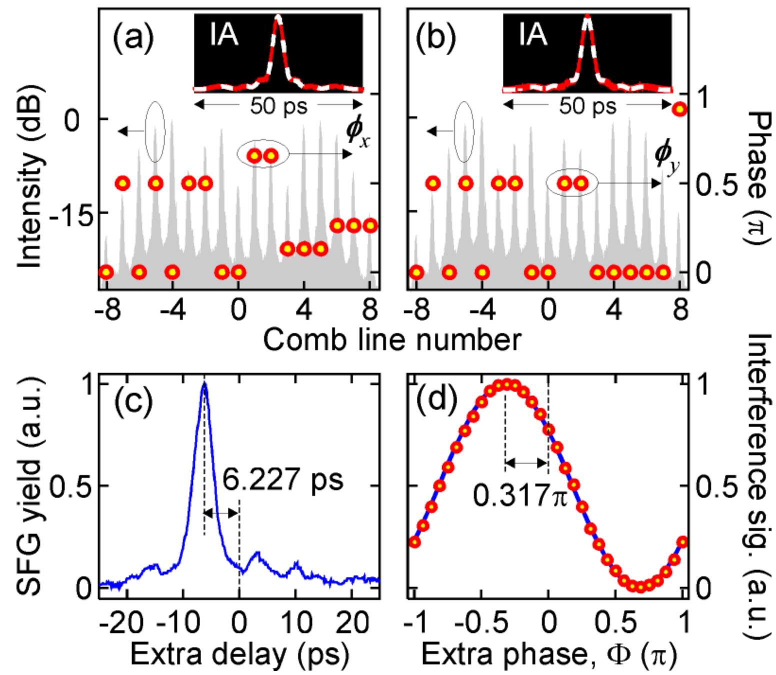

Fig. 3. The raw V-OAW measured by the four-step method. (a-b) Spectral intensities (shaded) and phases (circles) of (a) $A_x(\omega)$ and (b) $rA_y(\omega)$, respectively. The insets show the intensity-autocorrelation traces of x- and y-polarized TL pulses obtained by experiment (solid) and simulation (dashed), respectively. (c) Intensity cross-correlation trace between x- and y-polarized TL pulses for τ_{xy} measurement. (d) Interference signal $I_{45}(\omega_0)$ versus the extra phase Φ applied to the y-polarization used for θ measurement.

The polarization line-by-line pulse shaper in our setup enables independent measurement of $\boldsymbol{e}(t)$ by a 4-step method similar to that used in [1]. In Steps 1 and 2, $\phi_x(\omega)$ and $\phi_y(\omega)$ [Figs. 3(a) and 3(b)] were determined by maximizing the SHG yields of the x- and y-polarized combs, respectively (Fig. 1, Path-2B). The accuracy was verified by performing shaper-assisted intensity autocorrelation (IA) [24] for the phase-compensated transform-limited (TL) pulses at x- and y-polarizations (Fig. 1, Path-2B). The insets of Figs. 3(a) and 3(b) show that the experimentally measured IA functions (solid) are in good agreement with the simulated ones assuming TL pulses (dashed). In Step 3, the x- and y-polarized TL pulses were sent into the Type II BBO for shaper-assisted intensity cross-correlation to characterize τ_{xy} (Fig. 1, Path-1B). Figure 3(c) shows that the SFG yield was maximized when an extra delay of −6.227 ps was added to $e_y(t)$. The value of τ_{xy} is actually −6.277 ps by considering the 50 fs group velocity mismatch walk-off between the fundamental e-wave (y-polarization) and o-wave (x-polarization) in the Type II BBO [25]. In Step 4, all but the central comb lines of the x- and y-polarizations were blocked by the pulse shaper and the interference signal $I_{45}(\omega_0)$ [Fig. 3(d), circles] versus an extra phase $\Phi\in[-\pi,\pi]$ added to the y-polarization was recorded (Fig. 1, Path-2A). The interference signal peak reveals that the central comb line of the y-polarization differs from the x-counterpart by a phase of $\theta = 0.317\pi$. The spectral phases $\phi_x(\omega)$ and $\phi_{y,tot}(\omega)$ obtained by the 4-step method [Figs. 2(a) and 2(c), solid] agree well with those retrieved by VECTOR. The values of (τ_{xy},θ) are (−6.277 ps, 0.317π) (4-step method) and (−6.306 ps, 0.316π) (VEVTOR), respectively. This shows that VECTOR can accurately characterize V-OAW with greatly simplified configuration.

3.2 Measurement of τ_{xy} and θ

We then synthesized two specific V-OAWs by applying different modulation functions to the perfectly phase-compensated combs [i.e. $\phi_x(\omega) = 0$, $\phi_{y,tot}(\omega) = 0$]. In the first case, the *y*-polarization was phase-modulated by a first-order polynomial $\phi_{y1}(\omega) = \tau_{xy}\omega + \theta$ with (τ_{xy},θ) = (1 ps, 0.25π) (while the *x*-polarization was intact). Fitting the spectral phase $\phi_{y,tot}(\omega)$ retrieved by VECTOR [Fig. 4(c), circles] by a first-order polynomial accurately recovers (τ_{xy},θ) = (1.011 ps, 0.258π). The synthesized V-OAW [Fig. 4(d)] exhibits time-varying elliptical polarization with nearly constant instantaneous frequencies. To verify the measurement result, we acquired a MIIPS trace $S(\omega,\delta)$ [Fig. 4(a), left panel] by applying a variable sinusoidal phase function $2\pi \times \sin(\tau_m\omega + \delta)$ with τ_m = 1 ps, $\delta\in[-\pi,\pi]$ to the 45°-polarized field component (selected by the polarization manipulator) for SHG (Fig. 1, Path-2C). The root-mean-square error ε between the measured and calculated MIIPS traces $S(\omega,\delta)$ and $S'(\omega, \delta)$ (both are normalized to unit peak) is minimized when (τ_{xy},θ) = (± 1.02 ps, ± 0.266π) [Fig. 4(b), cross, diamond]. This is the first experimental demonstration that MIIPS trace is useful in vectorial field reconstruction though the sign ambiguity of (τ_{xy},θ) [when $A_x(\omega) = A_y(\omega)$ occurs] has to be removed by an extra measurement [19].

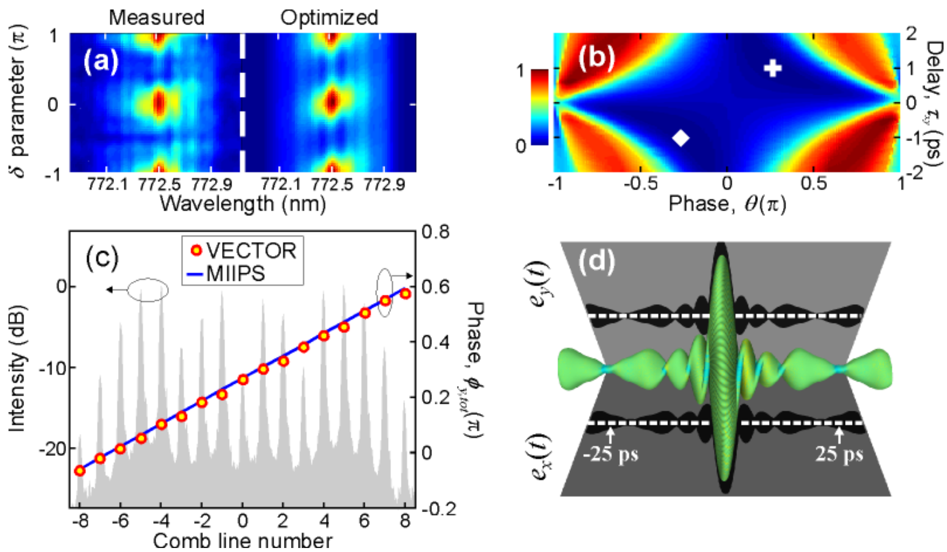

Fig. 4. Measurement of a V-OAW with $\phi_x(\omega) = 0$, $\phi_y(\omega) = 0$, τ_{xy} = 1 ps and θ = 0.25π. (a) The measured (left) and optimized (right) MIIPS traces of 45°-polarized field. The definition of δ-parameter is shown in the main text. (b) Error surface between the measured and calculated MIIPS traces at different combinations of (τ_{xy},θ). Two minima points are denoted by cross and diamond. (c) Spectral intensity $r^2|A_y(\omega)|^2$ (shaded) and phase $\phi_{y,tot}(\omega)$ obtained by VECTOR (circles) and minimization of MIIPS error (solid), respectively. (d) The quasi-3D representation of the VECTOR-reconstructed $\boldsymbol{e}(t)$.

3.3 Measurement of vectorial temporal Talbot effect

In the second case, we generated an intensity-rate doubled vectorial pulse train by applying periodic spectral phases of $\phi_{x2}(\omega)$ = {0, π/2} and $\phi_{y2}(\omega)$ = {π, π/2} [Figs. 5(a) and 5(b), solid] to the phase-compensated *x*- and *y*-polarized combs, respectively. The abrupt phase jumps were accurately resolved by VECTOR [Figs. 5(a) and 5(b), circles]. The resulting intensity-rate doubled *x*- and *y*-polarized pulses have pulse-by-pulse temporal phases of {0, −0.5π} and

#223524 - $15.00 USD Received 24 Sep 2014; revised 2 Nov 2014; accepted 3 Nov 2014; published 11 Nov 2014

{0.5π, −π}, respectively. The pulse-by-pulse phase difference of {-0.5π, 0.5π} between the two orthogonal polarizations results in alternating handedness for the vectorial field. The synthesized V-OAW [Fig. 5(c)] shows doubled (40 GHz) intensity repetition rate, while the fields around the time instants of 0 and ± 25 ps [Fig. 5(c), insets] exhibit left- and right-handed rotations, respectively. The instantaneous frequencies of the two synthesized V-OAW examples are nearly constant for the waveforms are almost chirp-free.

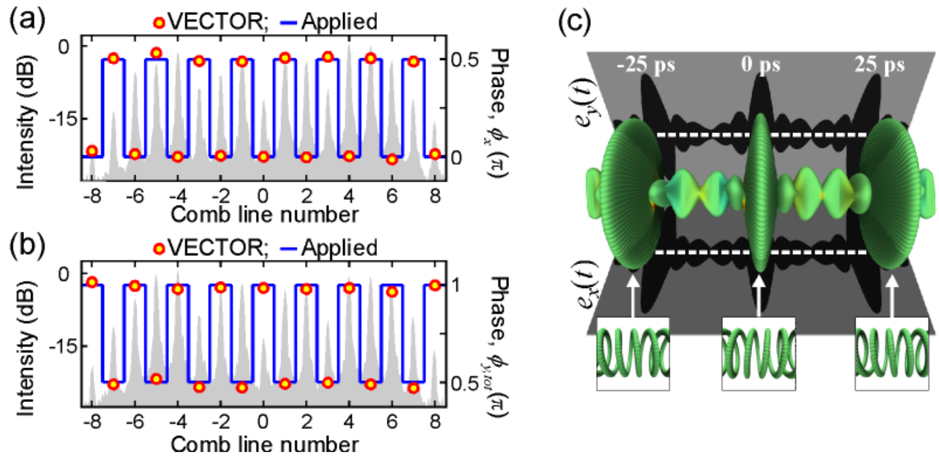

Fig. 5. Measurement of an intensity-rate doubled V-OAW. (a-b) Spectral intensity (shaded) and phase (circles) of (a) $A_x(\omega)$ and (b) $r|A_y(\omega)| \times \exp[j\phi_{y,tot}(\omega)]$, respectively. The $\phi_x(\omega)$ and $\phi_{y,tot}(\omega)$ applied by the pulse shaper are depicted (solid) for comparison. (c) The quasi-3D representation of the VECTOR-reconstructed $\boldsymbol{e}(t)$.

4. Conclusions

We demonstrated an integrated system that can simultaneously synthesize and characterize V-OAW (conceptually the optical field of extreme complexity in the time/frequency domain if a large number of comb lines are accessed) without RF or external optical reference, restriction on the comb spacing, and requirement of external interferometric stabilization. The field retrieval is non-iterative and unambiguous, only utilizing the data sets from one nonlinear measurement (DQ-SSI) and one linear measurement (WPP).

Acknowledgments

The authors gratefully thank C. B. Huang, A. H. Kung and A. M. Weiner for their technical support and valuable comments, respectively. This work was supported by the National Science Council of Taiwan under grant NSC 100-2221-E-007-093-MY3, and by the National Tsing Hua University under grant 102N2081E1.